



Contents lists available at ScienceDirect

Nuclear Instruments and Methods in Physics Research B

journal homepage: www.elsevier.com/locate/nimb

Effect of valence holes kinetics on material excitation in tracks of swift heavy ions

R.A. Rymzhanov^{a,*}, N.A. Medvedev^b, A.E. Volkov^{a,c,d}^a FLNR, JINR, Joliot-Curie 6, 141980 Dubna, Russia^b CFEL at DESY, Notkestr. 85, 22607 Hamburg, Germany^c NRC Kurchatov Institute, Kurchatov Sq. 1, 123182 Moscow, Russia^d LPI of the Russian Academy of Sciences, Leninskij prospekt, 53, 119991 Moscow, Russia

ARTICLE INFO

Article history:

Received 14 May 2015

Received in revised form 13 August 2015

Accepted 20 August 2015

Available online xxxx

Keywords:

Swift heavy ion track

Complex dielectric function

Monte Carlo

Aluminum oxide

Hole diffusion

ABSTRACT

A considerable part of the excess energy of the electronic subsystem of a solid penetrated by a swift heavy ion (SHI) is accumulated in valence holes. Spatial redistribution of these holes can affect subsequent relaxation, resulting in ionizations of new electrons by hole impacts as well as energy transfer to the target lattice. A new version of the Monte Carlo code TREKIS is applied to study this effect in Al_2O_3 for SHI tracks. The complex dielectric function (CDF) formalism is used to calculate the cross sections of interaction of involved charged particles (an ion, electrons, holes) with the target giving us ability to take into account collective response of a target to excitations.

We compare the radial distributions of the densities and energies of excited electrons and valence holes at different times to those obtained under the assumption of immobile holes used in earlier works. The comparison shows a significant difference between these distributions within the track core, where the majority of slow electrons and valence holes are located at femtosecond timescales after the ion impact. The study demonstrates that the energy deposited by valence holes into the lattice in nanometric tracks is comparable to the energy transferred by excited electrons. Radii of structure transformations in tracks produced by these energy exchange channels are in a good agreement with experiments.

© 2015 Elsevier B.V. All rights reserved.

1. Introduction

Swift heavy ions (SHI, $M \geq 20 m_p$, $E > 1 \text{ MeV/amu}$) decelerated in the electronic stopping regime lose their energy in solids predominantly (>95%) on excitation of the electron subsystem of the target, reaching up to $\sim 40 \text{ keV/nm}$ [1]. Subsequent relaxation of the excess energy of the electronic subsystem accompanied by energy transfer to the lattice may result in nanometric structure and phase transformations along the SHI trajectory [2,3].

Initially produced by an SHI impact, δ -electrons spread from the projectile trajectory dissipating the energy they possess on the femtosecond scale [4–6]. Evolution of the spectra of the excited electronic subsystem determines the kinetics of energy transformations resulting finally in excitation of the material and observable effects. Thus, detailed modeling of the transient kinetics of excited conduction-band electrons and valence-band holes in the nanometric vicinity of SHI trajectory is essential for understanding evolution of the target material properties during irradiation.

Recently, we have shown that the kinetics of valence band holes in insulators plays an important role in SHI track creation [7]. It was demonstrated that coupling of only the excited electrons to the lattice does not provide sufficient energy for a detectable structure transformations in SHI tracks. Only when the excess energy of valence band holes was included, the track radii formed in the modeling were similar to those found in experiments [8]. Therefore, the kinetics of valence band holes in relaxing SHI tracks must be studied in more detail. In particular, Ref. [7] as well as the majority of other works (see e.g. [9,10]) did not consider spatial redistribution of valence holes from the SHI trajectory. On the other hand, it was demonstrated in Ref. [11] that diffusion of created valence holes considerably changes their spatial profile and, therefore, the profile of the excess energy they contain, already on the picosecond timescale after an SHI passage.

In the present work we include the valence-band holes transport into the recently developed Monte Carlo code TREKIS [12]. The described approach is applied to Al_2O_3 , analyzing kinetics of the excited electron subsystem in SHI tracks. Radial distributions of electrons and holes and their energy densities around the ion trajectory in Al_2O_3 as well as the energy transferred to the lattice

* Corresponding author.

during the first 100 fs after passage of a Xe 167 MeV ion are calculated. The results are compared with those of application of the previous version of our model which did not include valence holes transport. The radial distribution of the energy transferred into the lattice is used as input data for classical molecular dynamics simulating subsequent relaxation of the lattice and structure transformations appearing near the ion trajectory. The results of MD simulation coincide well with the experimental data.

2. Model

Within the assumed first Born approximation, a cross section of scattering of an incident particle on dynamically coupled system of scattering centers can be factored into a product of the cross section of scattering on a single (isolated) center and the dynamic structure factor (DSF) [13], which takes into account a collective response of a target to an excitation. For scattering of charged particles, the DSF is then expressed in terms of the loss function (inverse imaginary part of the complex dielectric function, $\varepsilon(\omega, \mathbf{q})$) via the fluctuation–dissipation theorem [14,15]. This results in the following form of the differential cross section of a charged particle interaction with a solid [6]:

$$\frac{d^2\sigma}{d(h\omega)d(hq)} = \frac{2|Z_e(v, q)e|^2}{\pi\hbar^2 v^2} \frac{1}{\hbar q} \operatorname{Im} \left[\frac{-1}{\varepsilon(\omega, \mathbf{q})} \right], \quad (1)$$

where $Z_e(v, q)$ is the effective charge of the projectile penetrating through a solid as a function of its velocity, v , and transferred momentum, \mathbf{q} (for an incident electron $Z_e = 1$, for an SHI see the discussion about Z_e in [12]); $\hbar\omega$ is the transferred energy in the considered scattering event; \hbar is the Plank constant; e is the electron charge.

The CDF can be reconstructed from optical data (refractive index n and extinction coefficient k) in the form of a set of artificial oscillators [15]:

$$\operatorname{Im} \left[\frac{-1}{\varepsilon(\omega, q)} \right] = \sum_{i=1}^{n_{os}} \frac{A_i \gamma_i \hbar \omega}{\left[\hbar^2 \omega^2 - (E_{0i} + \hbar^2 q^2 / (2m_e)) \right]^2 + (\gamma_i \hbar \omega)^2}, \quad (2)$$

where the summation is running through all the oscillators n_{os} ; coefficients E_{0i} , A_i and γ_i are carefully chosen to reproduce the optical constants of these materials, which can be found in Ref. [16] for low-energy photons (<30 eV), or in Ref. [17] for photons of higher energies. The algorithm finding these coefficients is thoroughly described in Refs. [12,15,18]. Fitted parameters E_{0i} , A_i and γ_i for alumina were published in [4].

This method allows taking into account collective effects occurring in a solid during a charged particle scattering resolved by photo-absorption experiments [15], e.g. plasmon excitation as well as optical part of lattice collective vibrations (phonons) for an electron (or a hole) scattering.

In the present paper, we divide the reconstructed cross sections of the charged particle interaction with the solid into two nearly independent channels: elastic and inelastic scattering. The elastic interaction means the scattering of an incident particle on the target lattice. In contrast, inelastic processes result in ionization or excitation of target atoms generating new free electrons.

Finally, the calculated cross sections are implemented into asymptotic trajectory Monte Carlo code (TREKIS [12]) using the Poisson distribution for the free-flight distance [6,19] and the mean free path of a projectile scattering. The approach describes: (a) penetration of a swift heavy projectile resulting in ionization of a target and appearance of primary fast electrons (δ -electrons); (b) scattering of these fast electrons on lattice atoms and target electrons as well as the kinetics of all secondary generations of electrons arising during relaxation of the electron subsystem; (c) Auger decays, which are also resulting in produc-

tion of secondary electrons, as well as radiative decays of deep shell holes emitting photons (which is only a small effect for the energies and the material considered here).

During penetration of a charged particle, the target is assumed as homogeneous atom and electron arrangements with the densities corresponding to the solid densities of the materials, and no orientation effects are taken into account, such as channeling of the SHI. No defects or impurities in the material are included in these MC simulations.

Target electrons are considered as uniformly distributed particles occupying either the deep atomic energy levels [20] or the states in the valence or conduction bands according to the density of states (DOS) of a material (Al_2O_3 [21]). Taking into account large velocities of projectiles, we assume these electrons as point-like particles at fixed positions during their energy and momentum exchange with an SHI (instant collisions).

We assume that a scattering event of an incident electron on the target can result in appearance of only one new electron because multiple electron excitations by a single impact is much less probable. The energy transferred in the collision is determined from the differential cross sections given by Eq. (1). Because of the limited energies, neither ions nor the produced electrons manifest relativistic effects, Cherenkov, or Bremsstrahlung emissions. All the secondary electrons appearing in cascades are modeled in the same scheme as the primary ones.

3. Effect of valence holes motion

In the present work we improve our model TREKIS by including spatial redistribution of valence holes and their interaction with a target. This allows to study the effect of valence holes mobility on the kinetics of the material excitation and relaxation in an SHI track. The main goal of this consideration is to establish the role of valence holes redistribution in the processes of energy transfer from electron subsystem into the target lattice.

3.1. Kinetics of valence holes

We consider a hole as an independent point-like quasi-particle, which occupies an energy level E_h in the valence band, distributed according to the density of states of the material, $D(E)$. In order to realize the MC procedure, the knowledge about a dispersion relation $q(E)$ of the particle in the valence band is necessary. $q(E)$ can be determined from the density of states of the material within the ‘effective one-band’ approximation [22]:

$$D(E) = \frac{\sigma}{2\pi^2} q^2(E) \frac{dq}{dE}, \quad (3)$$

where σ determines the spin factor which is equal to two for the electron system. In the ‘effective one-band’ model [22], Eq. (3) can be solved analytically for the assumed isotropic momentum:

$$q(E) = \sqrt[3]{\frac{6\pi^2}{\sigma} \int_0^E d\varepsilon \cdot D(\varepsilon)} \quad (4)$$

which results in an average isotropic dispersion relation between the momentum q and the energy E . Introducing an effective mass of a hole, m_h^{eff} , this dispersion relation can be substituted by “free particle” dispersion relation $E_h = \hbar^2 q_h^2 / 2m_h^{\text{eff}}$, where m_h^{eff} now is a function of the hole energy (E_h). Using this effective mass, the velocity of a valence hole at a given energy state can be determined and implemented into Eq. (1) to calculate the partial cross sections of a hole interaction with a material. The differential cross section in Eq. (1) does not depend explicitly on the effective mass m^{eff} of an incident particle, but is inversely proportional to the squared velocity. Considering the dependence of these cross sections on

the kinetic energy of a projectile, one can reveal that $\frac{d^2\sigma}{d(h\nu)d(hq)}$ is directly proportional to m_e^{eff} .

Fig. 1 demonstrates the effective mass of valence holes calculated (Eq. (4)) from DOS of Al_2O_3 taken from [21]. The obtained average valence hole mass seems to be in a reasonable agreement with ab initio calculations, which estimated it to be $3.99 m_e$ [23].

Holes at the deep atomic shells (core holes) are assumed to be immobile and can relax via the Auger process or the radiative decay only.

Propagation of a valence hole describes the collective movement of VB electrons. This movement can occur without changing of an electronic energy state (ordinary propagation) or with change of a hole energy in the valence band. The latter processes are related to the interaction of the hole with target atoms: ionization or elastic scattering. Note that the impact ionization by a hole in dielectrics can only occur if the width of the valence band E_{VB} is larger than the width of the band gap E_{gap} , because the maximal hole energy E_h is restricted by E_{VB} [24]. $E_{gap} = 8.8 \text{ eV}$ in Al_2O_3 , thus impact ionization by a valence hole cannot be realized in this material.

In the present paper any interaction between electrons and holes is assumed to be small. The energy transfer is restricted in time by fast dissipation of the density of the excess electronic energy due to spatial spreading of electronic excitations from the ion trajectory (10–100 fs after the ion passage, see below). Therefore, mechanisms and processes working in the relaxing electronic subsystem at times larger than the time of spatial dissipation of the excess electronic energy do not affect the kinetics of lattice excitations in an SHI track.

Core holes produced due to ionization of deep atomic shells are immobile and locate in the closest vicinity ($<1 \text{ nm}$) of the ion trajectory. Such holes quickly decay via Auger (or interatomic Auger [25]) channel (1–10 fs), creating holes in the valence band. Taking this into account, we neglect the effect of Coulomb interaction of these core holes with electrons and valence holes appearing in an SHI track.

As will be shown below, delocalized valence holes have mobility in Al_2O_3 comparable to that of conduction band electrons. At the densities of valence holes and electrons produced in SHI tracks the lifetime of these holes is $\sim 1 \text{ ns}$ [26]. Taking into account the dissipation time of the density of the excess electronic energy there (10–100 fs), influence of the electron-hole recombination on the lattice heating can be neglected.

The mobility of valence holes and their interaction with electrons result in joint “charge neutral” diffusion of these particles. That is because in solids, in contrast to plasma, not only electrons

will be attracted backwards to the track center, but holes will also propagate outwards from the track core, forming the so-called ambipolar diffusion of electrons together with the valence-band holes. Therefore, in the first approximation the effect of interaction of valence holes and electrons may also be neglected describing lattice excitation in a SHI track (at least in alumina).

There can be an additional mechanism of relaxation of the excess electronic energy in wide band gap dielectrics: decay of excitons. The influence of this process on the lattice excitation in an SHI track in Al_2O_3 is negligible because the number of formed excitons is very small and its decay typically lasts nanoseconds.

Cross sections of a hole interaction with the target are calculated via the complex dielectric function formalism as described in Section 1.

Fig. 2 shows calculated mean free paths of electrons and holes as functions of the energy of particles measured from the Fermi level E_f for electrons, or from the top of the valence band for holes. The elastic mean free paths in Fig. 2 denote the interaction of incident particles with optical phonons. As discussed above, the CDF describing this kind of interaction can be extracted from the optical constants in the infrared region. The elastic mean free paths of the valence holes is a few times shorter than those of electrons resulting from the larger effective hole mass in this energy region (see Fig. 1).

Spatial propagation of valence hole is modeled in the same manner as for SHI or for electrons. The Monte Carlo procedure is described in the first section and in Refs. [4,12].

3.2. Effect on material relaxation

Fig. 3 demonstrates the densities of generated electrons and valence holes after a passage of Xe ion in Al_2O_3 . Valence holes do not affect the propagation of generated free electrons in SHI track, since we neglected the interaction between them, and also due to impossibility of ionizations by hole impacts in Al_2O_3 ($E_{gap} > E_{VB}$).

One can see from Fig. 3 that the change of holes density occurs at radii of several tens of angstroms, which is comparable with the typical size of a damaged region ($\sim 50 \text{ \AA}$) [11].

As was discussed in Ref. [7], it is experimentally known that Xe 167 MeV ion irradiation ($dE/dx = 24 \text{ keV/nm}$) in alumina can damage the area with transverse size of $\sim 1.3 \text{ nm}$ (13 \AA) around SHI trajectory [8]. Considering the density of the energy transferred to the lattice in the Xe ion track (Fig. 4, the filled blue squares) one finds that the energy deposited by free electrons is not sufficient to produce structure transformations [7]. Even at the times of cooling down of electrons due to spatial propagation ($\sim 100 \text{ fs}$), the density of the excess lattice energy in the track center ($R = 1\text{--}7 \text{ \AA}$) is only

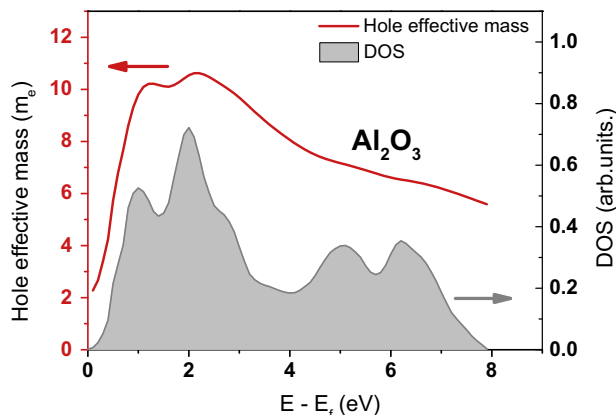


Fig. 1. Effective mass of valence holes calculated from the density of states (DOS) of Al_2O_3 .

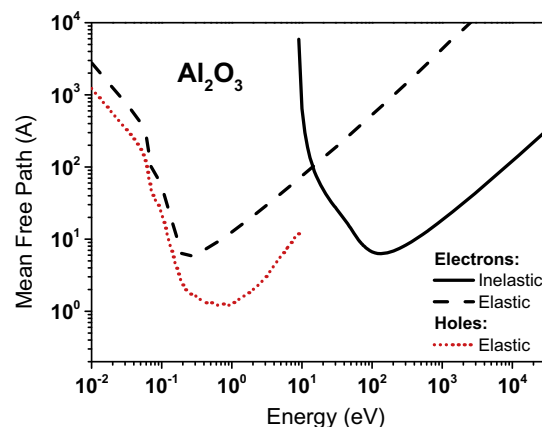


Fig. 2. Elastic and inelastic mean free paths of electrons and holes in Al_2O_3 .

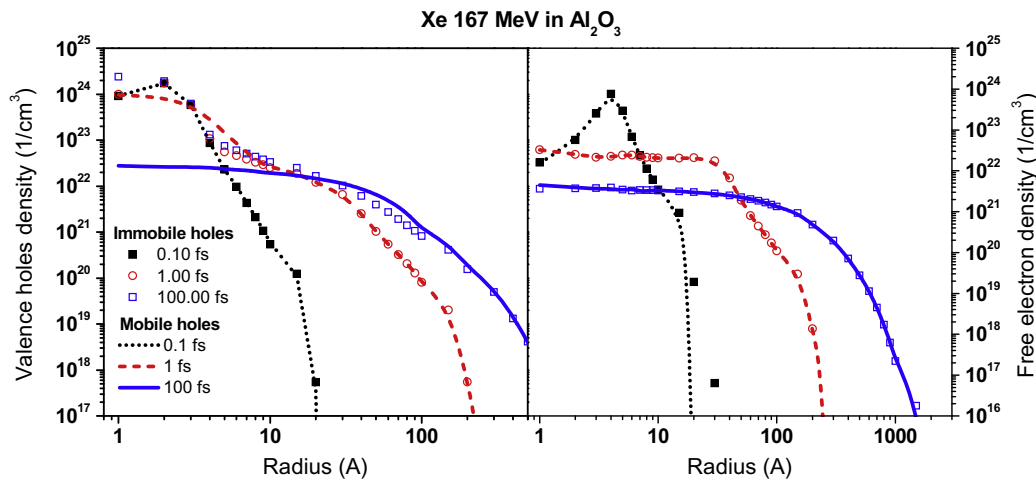


Fig. 3. Radial densities of valence holes (left panel) and ionized electrons (right panel) at different times after a passage of Xe 167 MeV in Al_2O_3 .

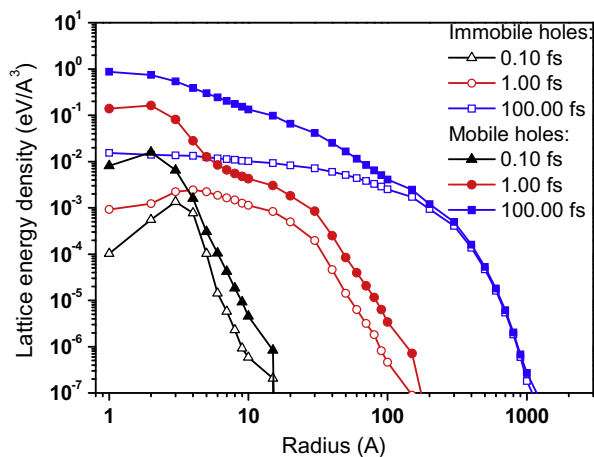


Fig. 4. Radial density of the lattice energy in track of Xe 167 MeV ion in Al_2O_3 .

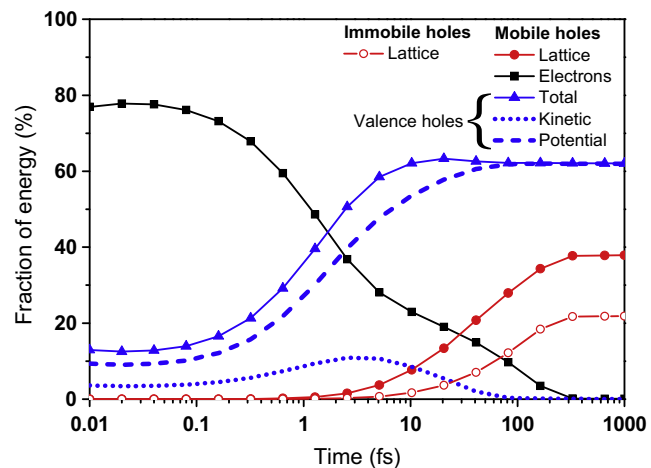


Fig. 5. Fractions of energy accumulated in each subsystem of a solid at different times in track of Xe 167 MeV ion in aluminum oxide.

about $0.01 \text{ eV}/\text{\AA}^3$, which corresponds to the lattice temperature of about 1000 K, whereas melting point of aluminum oxide is 2330 K [7]. It should be noted that in this paper we do not take into account any relaxation of energy accumulated in ion subsystem during this 100 fs, which results in slight overestimation of the lattice temperature.

The spatial redistribution of holes (filled symbols in Fig. 4) and their interaction with the lattice result in larger energy transfer to target atoms. According to Fig. 5 the energy deposited into the ion subsystem by valence holes can constitute up to 50% of total excess lattice energy integrated over all considered volume. It is worth to mention that in contrast to electrons, the valence holes transfer their energy to the lattice only in the narrow region (radius < 10 nm, Fig. 4) around SHI track, that causes the significant increase of lattice temperature in this region, while atomic temperature of the periphery almost does not change.

4. Atomic dynamics after SHI passage

For investigation of the valence holes contribution to the lattice excitation in an SHI track we use the model of instant deposition of the energy they accumulated to the atomic system at 100 fs after the ion impact followed by description of lattice relaxation by means of Molecular Dynamics using the classical MD code LAMMPS [27]. The interactions between atoms in Al_2O_3 are calcu-

lated using the Buckingham type potential developed by Matsui [28]. The total energy profile transferred to the lattice from free electrons and from the valence-band holes calculated with TREKIS (the filled blue squares in Fig. 4 at 100 fs after SHI impact) is used as the initial profile of the energy deposited into the lattice. 100 fs was chosen as the starting point for MD because at these times all secondary ionization cascades are finished and energy transfer to the target atoms reaches more than 85% of all the transferred energy.

The remaining energy of valence holes at 100 fs (Fig. 5) mainly consists of a potential energy of the electron–hole pairs and will not further heat the lattice. As discussed above, this part of the excess electronic energy will be released at the nanosecond time-scales after the ion passage [26]. These times are much longer than the characteristic times of electronic and atomic relaxation. The density of the energy transferred to the lattice due to decay of such electron–hole pairs is thus expected to be very low due to long-time diffusion.

We used corundum structure of Al_2O_3 (space group R-3c with lattice parameters (4.762, 4.762, 12.99, 90, 90, 120)), which consists of a distorted hexagonal close-packed oxide sublattice with Al^{3+} cations occupying two thirds of the available octahedral holes. The supercell size used in the MD simulations is chosen as $9.4 \times 9.7 \times 7.7 \text{ nm}^3$ with the periodic boundary conditions. The

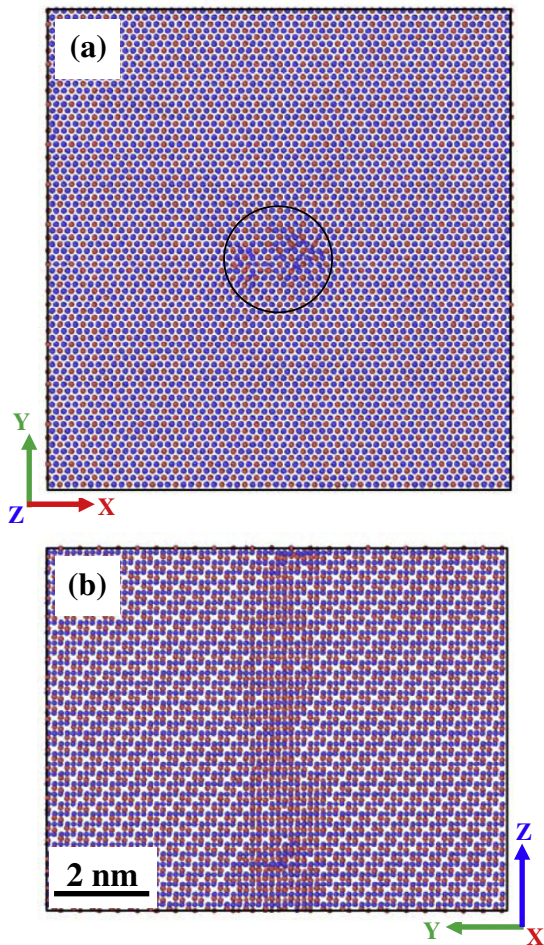


Fig. 6. Atomic snapshots of Al_2O_3 lattice in the nanometric vicinity of the trajectory of a 167 MeV Xe ion. Al atoms are red dots, O atoms are blue dots. (a) The projection along c-axis (Z) is [001] direction of the hexagonal cell, coinciding with the SHI trajectory; (b) the projection along a-axis (X) is [100] direction of the hexagonal cell. (For interpretation of the references to colour in this figure legend, the reader is referred to the web version of this article.)

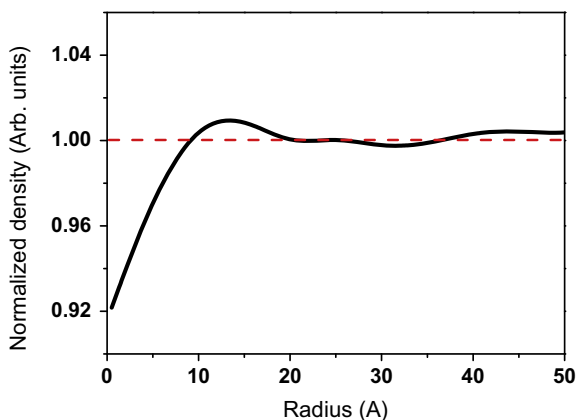


Fig. 7. Density of aluminum oxide vs. distance from the ion trajectory. The data are normalized to the density of the undamaged material.

borders of the computational cell (last 0.5 nm) in the X- and Y-directions are cooled by the Berendsen thermostat. Track evolution is traced up to 50 ps after the projectile passage. By this time the temperature of the supercell drops below 310 K, so no structural changes are expected after that.

Fig. 6 demonstrates the simulated shell after a passage of Xe ion with energy 167 MeV in Al_2O_3 . Relaxation of the excess energy of valence holes results in structure transformation with the average track diameter of ~ 1.6 nm. The experimental analysis of the track structure in Al_2O_3 is very complex due to small size of the track region (about 2–3 unit cell size [8]). However, it seems that Xe ion track in Al_2O_3 is crystalline and consists of a set of discontinuous regions with lower density, but not ‘voids’ in the conventional sense. In our MD picture we see the damaged region with varying transverse size at different depths. The density of central region is lower than the density of the undamaged material (Fig. 7), which allows us to conclude that our predictions are in qualitative agreement with the experiment.

Fig. 7 shows the radial dependence of the alumina density in the vicinity of Xe ion trajectory. At the very center of a track, the decrease of the density is about 7%, while the increase of the density in a so-called shell of SHI track is less than 1%.

5. Conclusions

In this paper we analyzed an effect of the valence holes mobility on track formation in Al_2O_3 after impact of a swift heavy ion decelerated in the electronic stopping regime. Initial ion penetration, excitation of the primary and all secondary generations of free electrons, Auger decays of core holes, as well as motion and scattering of valence-band holes were modeled with in-house Monte Carlo code TREKIS. Cross sections of a free electron and a valence-band hole were obtained within the complex dielectric function formalism; an effective-one band model for the band structure of valence holes is used. Calculated heating of atomic system resulted from valence holes elastic scattering appeared to be as important as free-electron scattering. Only taking into account both of this channels, we observed a track formation within molecular dynamics modeling. The resulting track radius is in a very good agreement with the experimental data.

Acknowledgements

Dr. V.A. Skuratov (JINR, Dubna, Russia) is acknowledged for helpful discussions on his experimental data.

The results of the work were obtained using computational resources of MCC NRC “Kurchatov Institute” (<http://computing.kiae.ru/>) and CICC LIT JINR (<http://lit.jinr.ru/>). Partial financial support from grants 13-02-1020, 15-02-02875, 15-58-15002 of Russian Foundation for Basic Research is acknowledged by A.E. Volkov.

References

- [1] J.P. Ziegler, U. Biersack, J.F. Littmark, *The Stopping and Range of Ions in Solids*, Pergamon Press, New York, 1985.
- [2] A.M. Stoneham, N. Itoh, *Appl. Surf. Sci.* 168 (2000) 186–193.
- [3] F.F. Komarov, *Phys. Usp.* 46 (2003) 1253–1282.
- [4] R.A. Rymzhanov, N.A. Medvedev, A.E. Volkov, *Nucl. Instr. Meth. Phys. Res. B* 326 (2014) 238–242.
- [5] N.A. Medvedev, A.E. Volkov, N.S. Shcheblanov, B. Rethfeld, *Phys. Rev. B* 82 (2010) 125425.
- [6] A. Akkerman, M. Murat, J. Barak, *Nucl. Instr. Meth. Phys. Res. B* 269 (2011) 1630–1633.
- [7] P.N. Terekhin, R.A. Rymzhanov, S.A. Gorbunov, N.A. Medvedev, A.E. Volkov, *Nucl. Instr. Meth. Phys. Res. B* 254 (2015) 200–204.
- [8] V.A. Skuratov, J. O’Connell, N.S. Kirilkin, J. Neethling, *Nucl. Instr. Meth. Phys. Res. B* 326 (2014) 223–227.
- [9] M. Toulemonde, C. Dufour, E. Paumier, *Phys. Rev. B* 46 (1992) 14362–14369.
- [10] M.I. Kaganov, I.M. Lifshitz, L.V. Tanatarov, *Sov. Phys. JETP* 4 (1957) 173.
- [11] N.A. Medvedev, A.E. Volkov, K. Schwartz, C. Trautmann, *Phys. Rev. B* 87 (2013) 104103.
- [12] N.A. Medvedev, R.A. Rymzhanov, A.E. Volkov, *J. Phys. D Appl. Phys.* 48 (2015) 355303.
- [13] L. Van Hove, *Phys. Rev.* 95 (1954) 249–262.
- [14] D. Pines, *Elementary Excitations in Solids*, W.A. Benjamin inc., New-York – Amsterdam, 1963.

- [15] R.H. Ritchie, A. Howie, *Philos. Mag.* 36 (1977) 463–481.
- [16] E.D. Palik, *Handbook of Optical Constants of Solids*, Academic Press, San Diego, 1985.
- [17] B.L. Henke, E.M. Gullikson, J.C. Davis, *At. Data Nucl. Data Tables* 54 (1993) 181–342.
- [18] A. Akkerman, T. Boutboul, A. Breskin, R. Chechik, A. Gibrekhterman, Y. Lifshitz, *Phys. Status Solidi B* 198 (1996) 769–784.
- [19] B. Gervais, S. Bouffard, *Nucl. Instr. Meth. Phys. Res. B* 88 (1994) 355–364.
- [20] J.A. Bearden, A.F. Burr, *Rev. Mod. Phys.* 39 (1967) 125.
- [21] P.W. Peacock, J. Robertson, *J. Appl. Phys.* 92 (2002) 4712.
- [22] B.Y. Mueller, B. Rethfeld, *Phys. Rev. B* 87 (2013) 035139.
- [23] J.E. Medvedeva, E.N. Teasley, M.D. Hoffman, *Phys. Rev. B* 76 (2007) 155107.
- [24] N. Medvedev, B. Rethfeld, *New J. Phys.* 12 (2010) 073037.
- [25] N.A. Medvedev, A.E. Volkov, B. Rethfeld, N.S. Shcheblanov, *Nucl. Instr. Meth. Phys. Res. Sect. B Beam Interact. Mater. Atoms* 268 (2010) 2870–2873.
- [26] M. Kirm, G. Zimmerer, E. Feldbach, A. Lushchik, C. Lushchik, F. Savikhin, *Phys. Rev. B* 60 (1999) 502–510.
- [27] S. Plimpton, *J. Comput. Phys.* 117 (1995) 1–19.
- [28] M. Matsui, *Geophys. Res. Lett.* 23 (1996) 395–398.